A Gust Soaring Controller for Small Uninhabited Gliders

Jack W. Langelaan
The Pennsylvania State University
University Park, PA USA 16802
jlangelaan@psu.edu

Portions of this work were presented at the 2008 AIAA Guidance, Navigation and Control Conference, Honolulu, HI USA and at the 2011 SSA Conference, Philadelphia PA USA

Abstract

The focus of this paper is on gust soaring: energy extraction from atmospheric turbulence by small- and mini- uninhabited aerial vehicles. A controller which superimposes a gust-dependent control input on a state-feedback derived control input is proposed. A genetic algorithm is used to obtain control gains and the optimal nominal trim state is described. Control laws are designed for both vertical sinusoidal gust fields as well as vertical and longitudinal Dryden gust fields. The optimal trim state and controller gains are shown to vary with gust intensity, and results of Monte Carlo simulations show significant energy savings for the gust soaring controller over a feedback-only controller.

Nomenclature

C_D	drag coefficient
C_L	lift coefficient
C_T	thrust coefficient
$\mathbf{D}$	drag force
E	specific total energy
g	magnitude of acceleration due to gravity
$\mathbf{g}$	gravity acceleration vector
h	height above ground
$\mathbf{K}_s$, $\mathbf{K}_w$	gain matrix for state, wind
$L_{(\cdot)}$	characteristic length for gust field
$\mathbf{L}$	lift force
$\mathbf{p}_i$	candidate controller
$\mathbf{P}$	population of candidate controllers
q	dynamic pressure
Q	pitch rate
$\mathbf{r}$	position vector
$\mathbf{T}$	thrust force
v_a	magnitude of airspeed
$\mathbf{v}$	airspeed vector
$w_{(\cdot)}$	component of wind vector
$\mathbf{w}$	wind vector
x	vehicle horizontal position
$\mathbf{x}$	state vector
z	vehicle vertical position (positive down)
α	angle of attack
δ_e	elevator deflection
Φ	power spectral density
γ	flight path angle
θ	pitch angle
ρ	air density
σ	intensity
Ω	spatial frequency
ω	angular velocity

Subscripts/superscripts

air	air mass-referenced
b	body-fixed frame
earth	Earth-referenced
i	vector/component expressed in inertial frame
nom	nominal (trim) condition
s	vector/component expressed in wind axes
u, *w*	longitudinal, vertical component
x, *z*	vector component

Introduction

A major handicap associated with small- and mini- Unmanned Aerial Vehicles (UAVs, here small refers to vehicles with wingspan ranging from 1 to 4 m and mass ranging from 1 to 10 kg) is their limited on-board energy capacity (either as chemical fuel or as batteries). The reduced endurance and range that results greatly reduces the utility of such vehicles. Additionally, the low Reynolds numbers inherent to small UAVs make it difficult to achieve lift/drag ratios comparable to larger aircraft, further reducing overall performance.

However, significant energy is available from the atmosphere. Large birds and human sailplane pilots routinely exploit vertical air motion (lift) to remain aloft for several hours and fly hundreds of kilometers without flapping wings or the use of engines.

There are three sources of energy available from the atmosphere: (a) vertical air motion, such as thermal instabilities, orographic lift or wave; (b) non-stochastic spatial wind gradients, such as shear layers; (c) stochastic spatial or temporal gradients, such as gusts. Each source of energy operates on a different time scale and different assumptions are applicable to each case. Vertical air motion is generally long in duration compared with vehicle dynamics; hence a kinematic model for

the vehicle is sufficient. Exploitation of spatial gradients generally assumes that the wind field is known, and energy extraction is treated as a trajectory optimization problem. Further, the scale of the gradients is such that a point mass model is generally an adequate representation of vehicle dynamics. Temporal gradients (gusts) are short duration and a full dynamic model of the vehicle is necessary. Further, gusts are stochastic in nature, so accurate predictions of wind field are impossible.

The focus of this paper is on gust soaring. It has been observed by radio control glider pilots that flight performance relative to birds is significantly reduced on a gusty day[1]. This implies that birds are exploiting gusts to minimize the effect on performance (and, in fact, may be able to improve performance), a feat which human RC pilots are not able to reproduce. Kiceniuk reports that it is even possible to extract energy from a downward gust[2]!

While a significant amount of work has been done on exploiting longer-duration atmospheric effects (for example the autonomous soaring research described by Allen[3]) and dynamic soaring (i.e. exploiting spatial gradients in a wind field[1]) less work has been performed on exploiting gusts. Phillips describes an approach to compute an equivalent thrust coefficient that occurs due to vertical gusts[4], and concludes that the effect is too small to be useful in crewed aircraft. However, extending Phillips' approach to small UAVs shows that a significant performance improvement is possible.

Previous and related research

Driven by competition glider flying, a significant amount of work has been reported on optimal piloting techniques for static soaring. One of the most famous (and certainly most widely adopted) techniques was described by MacCready[5], which describes what is now known as MacCready speed to fly theory. Other selected examples include Arho[6], who examined minimum time soaring with a minimum altitude constraint; Metzger[7], who described maximum speed with no net altitude loss; de Jong[8], who discussed a geometric approach to sailplane trajectory optimization, and, more recently, Cochrane[9], who extends MacCready theory to uncertain lift.

The trajectory optimization literature generally uses a simplified glider model, which assumes that the pilot has direct control of airspeed. This assumption certainly is appropriate for long duration flights where the glider spends most of its time in a trimmed condition, but this assumption is not valid for periods of transition between trimmed conditions. Some authors have addressed optimal transitions to minimize energy loss[10, 11], and Gedeon[12] describes an analysis of "dolphin-style" flight through thermals.

Dynamic soaring by both aircraft and birds has again become an active area of research. Zhao[13] describes optimal trajectories for energy extraction from wind gradients and minimum fuel trajectories for power-assisted dynamic soaring are described by Zhao and Qi[14]. Dynamic soaring using shear layers is described by Sachs[15]. Elsewhere, he discusses the minimum wind shear strength required for albatross flight[16]. Pennycuick proposes an alternate flight mode where most of the energy gain is obtained from the shear layer which results from the wind's flow separation over the crest of each wave[17]. Successful exploitation of this strategy requires sensing very small changes in dynamic pressure, and he suggests that only tube-nosed birds such as albatrosses have the necessary sensory capability.

Both energy extraction from thermals and dynamic soaring are generally treated as deterministic problems. Gusts are inherently stochastic, are much shorter in duration, and generally show far greater spatial variation. This makes effective energy extraction more difficult. In addition, since useful energy extraction from gusts is only practical for small UAVs, it has received comparatively less attention. Works by Lissaman[18], Patel[19] and Lissaman and Patel[20] use a point mass model for the aircraft, thus ignoring potentially important dynamics (direct control of lift coefficient is used to enable energy harvesting). Previous work by Langelaan and Bramesfeld also uses vertical gusts, but a full dynamic model of aircraft longitudinal motion was used to generate control laws that maximized energy gain for flight through sinusoidal gusts[21]. This paper examines energy harvesting from both longitudinal and vertical gusts using elevator control.

Vehicle kinematics and dynamics

Only longitudinal motion is considered here. Consider an aircraft located at $\mathbf{r}$ in an inertial frame I, where $\hat{x}^i$ and $\hat{z}^i$ define unit vectors (see Figure 1).

$$\dot{\mathbf{r}} = \mathbf{v} + \mathbf{w} \qquad [1]$$

Hence

$$\ddot{\mathbf{r}} = \frac{d}{dt}\mathbf{v} + \frac{d}{dt}\mathbf{w} \qquad [2]$$

The angle γ defines the rotation between the wind axes and the inertial axes, and it is the flight path angle with respect to the surrounding air mass. When $\mathbf{w} = 0$ it is also the flight path angle with respect to the inertial frame. In this application γ is defined as positive upwards, so for a steady glide the glide slope is negative. The acceleration of the aircraft is

$$\frac{d}{dt}\mathbf{v} = \dot{v}_a\hat{x}^s + \omega^s \times v_a\hat{x}^s \qquad [3]$$

Substituting $\omega^s = \dot{\gamma}\hat{y}^s$ gives

$$\frac{d}{dt}\mathbf{v} = \dot{v}_a\hat{x}^s - \dot{\gamma}v_a\hat{z}^s \qquad [4]$$

Therefore

$$\mathbf{L}+\mathbf{D}+m\mathbf{g}+\mathbf{T}=m\left[\dot{v}_a\hat{x}^s-\dot{\gamma}v_a\hat{z}^s+\frac{d}{dt}\mathbf{w}\right] \quad [5]$$

Using standard expressions for coefficients and explicitly defining the coordinate frames used to express each force,

$$\mathbf{L}=-qSC_L\hat{z}^s \quad [6]$$

$$\mathbf{D}=-qSC_L\hat{x}^s \quad [7]$$

$$\mathbf{T}=qSC_T\hat{x}^b \quad [8]$$

$$\mathbf{g}=g\hat{z}^i \quad [9]$$

where $q=\frac{1}{2}\rho v_a^2$. The kinematics of the aircraft now can be defined in terms of the airspeed, flight path angle and wind speed. From the standpoint of control, it is generally more convenient to work in terms of pitch angle and angle of attack; Figure 1 shows that $\gamma=\theta-\alpha$:

$$\dot{x}_i=v_a\cos(\theta-\alpha)+w_x \quad [10]$$

$$\dot{z}_i=-v_a\sin(\theta-\alpha)+w_z \quad [11]$$

$$\dot{\theta}=Q \quad [12]$$

Vehicle dynamics are written in wind axes as

$$\dot{v}_a=\frac{qS}{m}(C_T\cos\alpha-C_D)-\frac{dw_x}{dt}\cos(\theta-\alpha)+\left(\frac{dw_z}{dt}-g\right)\sin(\theta-\alpha) \quad [13]$$

$$\dot{\alpha}=Q-\frac{qS}{v_am}(C_L+C_T\sin\alpha)-\frac{1}{v_a}\frac{dw_x}{dt}\sin(\theta-\alpha)-\frac{1}{v_a}\left(\frac{dw_z}{dt}-g\right)\cos(\theta-\alpha) \quad [14]$$

$$\dot{Q}=\frac{qSc}{I_{yy}}C_m \quad [15]$$

Aerodynamic coefficients are

$$C_L=C_{L0}+C_{L_\alpha}\alpha+\frac{c}{2v_a}\left(C_{L_Q}Q+C_{L_{\dot{\alpha}}}\dot{\alpha}\right)+C_{L_{\delta_e}}\delta_e+C_{L_{\delta_f}}\delta_f \quad [16]$$

$$C_D=f_{LD}\left(C_{L0}+C_{L_\alpha}\alpha\right)+C_{D_{\delta_e}}\delta_e+C_{D_{\delta_f}}\delta_f \quad [17]$$

$$C_m=C_{m0}+C_{m_\alpha}\alpha+\frac{c}{2v_a}C_{m_Q}Q+C_{m_{\delta_e}}\delta_e+C_{m_{\delta_f}}\delta_f \quad [18]$$

where $f_{LD}\left(C_{L0}+C_{L_\alpha}\alpha\right)$ is a polynomial function that relates drag coefficient to lift coefficient. Control inputs are thrust coefficient C_T, elevator deflection δ_e and flap deflection δ_f. While the thrust term is carried through in the derivation, later it will be set to zero to reflect gliding flight.

In a frozen (i.e. non time-varying) wind field, the rate of change of wind (wind acceleration) experienced by the aircraft is due to the spatial gradient and vehicle velocity, so that

$$\frac{d}{dt}\mathbf{w}=\nabla\mathbf{w}\begin{bmatrix}\dot{x}_i\\ \dot{z}_i\end{bmatrix}=\begin{bmatrix}\frac{\partial w_x}{\partial x_i}\dot{x}_i+\frac{\partial w_x}{\partial z_i}\dot{z}_i\\ \frac{\partial w_z}{\partial x_i}\dot{x}_i+\frac{\partial w_z}{\partial z_i}\dot{z}_i\end{bmatrix} \quad [19]$$

where $\nabla\mathbf{w}$ is the spatial gradient of the wind vector. Equivalently,

$$\frac{d}{dt}\mathbf{w}=\nabla\mathbf{w}\begin{bmatrix}v_a\cos(\theta-\alpha)+w_x\\ -v_a\sin(\theta-\alpha)+w_z\end{bmatrix}=\nabla\mathbf{w}\begin{bmatrix}v_a\cos(\theta-\alpha)\\ -v_a\sin(\theta-\alpha)\end{bmatrix}+\nabla\mathbf{w}\begin{bmatrix}w_x\\ w_z\end{bmatrix} \quad [20]$$

The kinematics and dynamics now can be used to find expressions for total energy and the rate of change of total energy.

Total energy

The choice of velocity reference (Earth or air mass) affects both the expression for total energy and total power.

Earth-referenced total energy

Relative to the Earth (assumed to be an inertial reference frame), specific total energy (energy divided by mass) is

$$E_{earth}=gh+\frac{\left(\dot{x}_i^2+\dot{z}_i^2\right)}{2} \quad [21]$$

Substituting kinematics (Equations 10 and 11),

$$E_{earth}=gh+\frac{1}{2}\left(v_a^2+2w_xv_a\cos\gamma-2w_zv_a\sin\gamma+w_x^2+w_z^2\right) \quad [22]$$

where for convenience $\gamma=\theta-\alpha$ is used. Specific total power is found by taking the time derivative:

$$\dot{E}_{earth}=g\dot{h}+\dot{v}_a\left(v_a+w_x\cos\gamma-w_z\sin\gamma\right)-v_a\dot{\gamma}\left(w_x\sin\gamma+w_z\cos\gamma\right)+\dot{w}_x\left(v_a\cos\gamma+w_x\right)+\dot{w}_z\left(-v_a\sin\gamma+w_z\right) \quad [23]$$

Substituting dynamics (Equations 13 and 14), recognizing that $v_a\dot{\gamma}=v_a\left(Q-\dot{\alpha}\right)$,

$$\dot{E}_{earth}=g\dot{h}+\frac{qS}{m}\left(-C_D+C_T\cos\alpha\right)\left(v_a+w_x\cos\gamma-w_z\sin\gamma\right)-\frac{qS}{m}\left(C_L+C_T\sin\alpha\right)\left(w_x\sin\gamma+w_z\cos\gamma\right)+g\left(-v_a\sin\gamma+w_z\right) \quad [24]$$

Finally, substituting $\dot{h} = -\dot{z} = v_a \sin(\theta - \alpha) - w_z$, specific total power relative to the inertial frame is

$$\dot{E}_{earth} = \frac{qS}{m}(-C_D + C_T \cos\alpha)(v_a + w_x \cos\gamma - w_z \sin\gamma) - \frac{qS}{m}(C_L + C_T \sin\alpha)(w_x \sin\gamma + w_z \cos\gamma) \quad [25]$$

Note that the above expression can also be derived from $\dot{E}_{earth} = \frac{(\mathbf{L}+\mathbf{D})\cdot(\mathbf{v}+\mathbf{w})}{m}$. This approach is used by Gorisch[22].

Wind gradients do not appear explicitly in the expression for total power expressed with respect to the inertial frame. Note, however, that time- and spatially-varying winds will result in time varying forces (through changes in airspeed and angle of attack), so wind gradients will indirectly affect total power.

Air mass-referenced total energy

It is more common in aircraft applications to write total energy with velocity expressed relative to the air mass, a non-inertial reference frame.

$$E_{air} = gh + \frac{v_a^2}{2} \quad [26]$$

The rate of specific total energy is

$$\dot{E}_{air} = g\dot{h} + v_a \dot{v}_a \quad [27]$$

Substituting dynamics gives

$$\dot{E}_{air} = g\dot{h} + \frac{qS}{m}(-C_D + C_T \cos\alpha)v_a - \dot{w}_x v_a \cos(\theta - \alpha) + \dot{w}_z v_a \sin(\theta - \alpha) - v_a g \sin(\theta - \alpha) \quad [28]$$

Recognizing that $\dot{h} = -\dot{z} = v_a \sin(\theta - \alpha) - w_z$,

$$\dot{E}_{air} = -gw_z + \frac{qS}{m}(-C_D + C_T \cos\alpha)v_a - \dot{w}_x v_a \cos(\theta - \alpha) + \dot{w}_z v_a \sin(\theta - \alpha) \quad [29]$$

Substituting the frozen wind field, the rate of change of total energy is

$$\dot{E}_{air} = -gw_z + \frac{qS}{m}(-C_D + C_T \cos\alpha)v_a - \mathbf{v}_a^T[\nabla\mathbf{w}]\mathbf{v}_a - \mathbf{v}_a^T[\nabla\mathbf{w}]\mathbf{w} \quad [30]$$

where $v_a = \begin{bmatrix} v_a \cos(\theta - \alpha) & -v_a \sin(\theta - \alpha) \end{bmatrix}^T$.

The contributions to the rate of change of total energy are immediately visible. The first term on the right hand side of Equation 30 is due to vertical air motion; the second term is energy lost due to drag or gained due to thrust[a]; and the last two terms show the effect of wind gradients on rate of change of energy. These last two terms enable dynamic and gust soaring. Typically airspeed is larger in magnitude than wind speed, so the third term will be more important than the fourth. It will contribute to energy gain under two conditions: first, when both $\nabla\mathbf{w}$ and $\gamma = \theta - \alpha$ are negative; second, when both are positive. For *steady* gliding flight the air mass relative flight path angle is always negative.

Comparing Earth- and air mass-referenced total power

When winds are constant (i.e. $\dot{\mathbf{w}} = 0$ and $\nabla\mathbf{w} = 0$), the air mass frame is an inertial reference frame. Under these conditions, it can be shown that the air mass-relative total power is equal to the Earth-reference total power. In a glide ($C_T = 0$) in constant wind, rearranging [25] gives

$$\dot{E}_{earth} = -\frac{qS}{m}C_D v_a + \frac{qS}{m}\left[-w_x(C_D \cos\gamma + C_L \sin\gamma) + w_z(C_D \sin\gamma + C_L \cos\gamma)\right] \quad [31]$$

In a steady glide $-\tan\gamma = \frac{C_D}{C_L}$, hence

$$C_D \cos\gamma + C_L \sin\gamma = 0.$$

Further, referring to Figure 1, $L\cos\gamma - D\sin\gamma = mg$. Thus $qS(C_D \sin\gamma - C_L \cos\gamma) = -mg$. For a steady glide in steady wind,

$$\dot{E}_{earth}\big|_{steady} = -gw_z - \frac{qS}{m}C_D v_a = \dot{E}_{air}\big|_{steady} \quad [32]$$

Hence, for steady (constant speed) flight in steady (non spatially or temporally varying) wind, the choice of reference frame is arbitrary.

The effect of wind gradients on energy change

Examining Equations 27 and 13 shows that wind gradients affect energy change through the vehicle dynamics (i.e. through the rate of change of airspeed). An estimate of the amount of energy that can be gained from gradients was obtained by examining energy gained from a sinusoidally varying vertical wind field, i.e.

$$w_z = w_{z,0} \sin\left(\frac{2\pi x}{L}\right) \quad [33]$$

In this case the rate of change of total energy (for gliding flight) is

[a] Although this will be accompanied by a loss in on-board stored energy, which is not explicitly accounted for here.

$$\begin{aligned}\dot{E}_{air} &= -gw_z - \frac{qS}{m}C_D v_a + v_a^2 \cos\gamma \sin\gamma \frac{dw_z}{dx} \\ &= -gw_z - \frac{qS}{m}C_D v_a + v_a^2 \cos\gamma \sin\gamma \frac{2\pi}{L} w_{z,0} \cos\left(\frac{2\pi x}{L}\right)\end{aligned} \quad [34]$$

The contribution of wind gradient to energy change is maximized when flight path angle $\gamma = \theta - \alpha$ is 45°, hence the largest possible contribution of wind gradient to energy change (i.e. the maximum value of the third term on the right hand side of Equation 34) is $\frac{\pi}{L} v_a^2 w_{z,0}$. Comparing this with the peak contribution of wind speed to energy change (the $-gw_z$ term in Equation 34) shows that the contribution of wind gradient to energy change is equal to the contribution of wind speed when $\frac{\pi v_a^2}{Lg} = 1$. If the gust wavelength is 50m this occurs when $v_a \approx 12$ m/s: this is well within the typical flight speed range of a small UAV. Clearly, as gust wavelength gets shorter the necessary airspeed is reduced. This assumes that the aircraft can react quickly enough that flight path angle can be regulated appropriately.

Energy maximization

Earlier research by several authors (previously cited), demonstrations by radio-controlled glider pilots and evidence from albatross flight shows that energy can be gained from gradients. Thus, it is necessary to consider air mass-reference total energy when dynamic or gust soaring is attempted. This matches intuition of course, since aerodynamic forces are a function of air mass relative speed and not inertial speed. Therefore, air mass referenced total energy will be used from this point forward, and for compactness the subscript will be dropped.

The choice of cost function has a tremendous impact on both mission performance and the final trajectory or control policy. Rather than maximize the rate of change of total energy, this paper works to maximize $\frac{\Delta E}{\Delta x}$, the change in specific total energy with respect to distance traveled. Clearly, in gliding flight in still air this quantity will be negative, representing energy loss. For gliding flight $C_T = 0$ and $\frac{dE}{dx} = \frac{\dot{E}}{\dot{x}}$:

$$\begin{aligned}\frac{dE}{dx} = \frac{1}{v_a \cos\gamma + w_x}\Bigg[&-gw_z - \frac{qS}{m}C_D v_a \\ &- \mathbf{v}_a^T \left[\nabla \mathbf{w}\right] \mathbf{v}_a - \mathbf{v}_a^T \left[\nabla \mathbf{w}\right] \mathbf{w}\Bigg]\end{aligned} \quad [35]$$

Unfortunately, simply computing some combination of airspeed and lift coefficient that maximizes the instantaneous value of $\frac{dE}{dx}$ results in "pushing the nose down" to maximize airspeed. To obtain a useful solution, one must compute a sequence of optimal airspeed, lift coefficient and flight path angle inputs over some finite time horizon (e.g. one period of a sinusoidal gust, as in Lissaman and Patel[20]). However, in the case of a stochastic gust field, this knowledge is unavailable, and a different approach that does not require knowledge of the full gust field is required.

Rather than controlling lift coefficient through flap deployment (as done by Patel and Kroo[19] and Patel [25]), here the focus is on controlling flight path and airspeed through elevator deflection. Note that this is not an attempt to control lift directly (although this will of course occur through changes in angle of attack). Another key difference with Patel and Kroo's work is that only vertical wind speed is used in computing the required C_L; here both wind speed and wind gradient is used to compute control surface deflection. Simultaneous control of flaps and elevator (i.e. controlling both lift and flight path) is left for future work.

A gust soaring controller

The problem is to find a closed-loop control law to maximize energy gain for flight through longitudinal and vertical gusts. This control law takes the form

$$\delta_e = \mathbf{K}_s \left[\mathbf{x}_{nom} - \mathbf{x}\right] + \mathbf{K}_w \begin{bmatrix} w_x \\ w_z \\ \frac{dw_x}{dx} \\ \frac{dw_z}{dx} \end{bmatrix} + \delta_e^{trim} \quad [36]$$

This is a linearized control law that regulates the state to some nominal trim condition and adds a feed forward term based on the wind condition. A block diagram is shown in Figure 2. In steady winds (i.e. zero gradient) appropriate choice of gains would result in trim at a condition that optimizes airspeed for a particular wind speed.

This approach has some key advantages over receding horizon control methods. It only requires knowledge of the wind field at the vehicle location, which in principle can be computed using on-board sensors such as GPS and air data. Depending on the choice of state gain $\mathbf{K}_s$ this system can guarantee closed-loop stability in the absence of gusts and the gain $\mathbf{K}_w$ enables energy extraction via deflection of the control surface (here only elevator is used, but one can add flaps or other control surfaces if they are available). In effect, control deflections that enable energy extraction are a perturbation superimposed on the control deflections made to maintain steady flight. This should allow non-steady flight (e.g. non-zero values of pitch rate Q or non-zero values of $\dot{v}_a$) to contribute to energy extraction.

Control of elevator deflection avoids problems associated with assuming the availability of direct control of lift coeffi-

cient (although flap deflection could be added to the control law if available).

Note that the control law proposed in [36] assumes that local wind speed and wind gradient is known. Methods for estimating wind speed using sensors typically available on small UAVs are discussed elsewhere (see for example Pachter et al.[28] or Myschik et al.[29]).

Control design procedure

Now, it remains to determine values for $\mathbf{x}_{nom}$, $\mathbf{K}_s$, and $\mathbf{K}_w$ which maximize energy gain. Since

$$\mathbf{x}_{nom} = \begin{bmatrix} \theta_{nom} & v_{a,nom} & \alpha_{nom} & Q_{nom} \end{bmatrix}^T \quad [37]$$

is a steady, trimmed glide state (with pitch rate $Q_{nom} = 0$), it is completely determined by airspeed.

Energy gain is likely to be a highly non-convex function of the controller parameters, thus gradient-based methods likely will converge to a local, rather than a global, optimum. Here a genetic algorithm is used to find the optimal energy extracting controller. Clearly, a genetic algorithm is not guaranteed to find the optimal controller, but it should find a good controller.

The procedure is shown in Figure 2. A candidate controller consists of a nominal airspeed and controller gains:

$$\mathbf{p}_i = \begin{bmatrix} v_{a,nom} & \mathbf{K}_s & \mathbf{K}_w \end{bmatrix} \quad [38]$$

and the population consists of the set of candidate controllers $\mathbf{P} = \{\mathbf{p}_i,\ i = 1 \ldots N\}$. The population is initialized with random candidate controllers, with $v_{a,nom}$ varying between stall speed and maximum speed. The state control $\mathbf{K}_s$ is checked to ensure that it is stabilizing for system dynamics linearized about best L/D speed before it is added to the population.

For each generation, the aircraft is flown through a gust field with each candidate controller and the objective function of Equation 33 is evaluated over the distance flown. Each candidate is given fitness

$$f_i = \begin{cases} \exp\dfrac{\Delta E}{\Delta x} & \text{if } \mathbf{x}_{\min} < \mathbf{x}_k < \mathbf{x}_{\max}\ \forall k \\ -9999 & \text{otherwise} \end{cases} \quad [39]$$

Candidates with $f_i = -9999$ are culled and, then, a minimum variance sampling algorithm[23] is used to select a new population with likelihood proportional to each candidate's fitness. Cross over and mutation occurs within this population to generate a new set of candidate controllers and the process repeats until convergence.

A new gust field is computed for each generation, thus ensuring that a "lucky" gust field does not adversely affect final results. A candidate controller that survives over multiple generations, thus, has shown good performance over several gust fields.

Gust fields

A stationary wind field can be represented as a sum of sinusoids[24]:

$$w(x) = w_0 + \sum_{n=1}^{N} a_n \sin(\Omega_n x + \varphi_n) \quad [40]$$

Random values of the phase φ_n simulate the random process and the choice of amplitude a_n defines the power spectral density.

While it is not clear that the Dryden gust spectrum is a good model for low altitude turbulence (especially for very small aircraft), it has been used by other researchers[19, 25] and it is used here as well. The power spectral density of the Dryden gust field is defined as[26]

$$\Phi_u(\Omega) = \sigma_u^2 \frac{2L_u}{\pi} \frac{1}{1 + (L_u\Omega)^2} \quad [41]$$

$$\Phi_w(\Omega) = \sigma_w^2 \frac{L_w}{\pi} \frac{1 + 3(L_w\Omega)^2}{\left(1 + (L_w\Omega)^2\right)^2} \quad [42]$$

For low altitudes (below 1000 feet) the length scale of the vertical gust is $L_w = h$ and the turbulence intensity is $\sigma_w = 0.1 w_{20}$, where w_{20} is the wind speed at 20 feet altitude. Horizontal gust length scale and intensity are related to the vertical scale and intensity by

$$\frac{L_u}{L_w} = \frac{1}{(0.177 + 0.000823h)^{1.2}} \quad [43]$$

$$\frac{\sigma_u}{\sigma_w} = \frac{1}{(0.177 + 0.000823h)^{0.4}} \quad [44]$$

where h is altitude in feet. The amplitude of a sinusoid in Eq. [40] is computed as

$$a_n = \sqrt{\Delta\Omega_n \Phi(\Omega_n)} \quad [45]$$

Gust soaring controllers

First, the design procedure described earlier is applied to a sinusoidal vertical gust field with wavelength 50m and several values of root mean square velocity. This provides a rough indication of convergence characteristics and will allow comparison with earlier results[21, 25].

Results showing best nominal airspeed and best energy extraction at each generation are plotted in Figure 3. After approximately 10 generations, the energy change converged to its final value. The trim airspeed takes somewhat longer to converge (and remains "noisier"), indicating that the cost function is likely to be rather flat near the optimum.

Increasing root mean square gust velocity results in higher nominal airspeeds and higher energy extraction. Net zero en-

ergy loss occurs when the root-mean-square gust velocity is approximately 1.5m/s, which agrees with results earlier obtained using a state tracking controller combined with optimal state computation using a steady state approximation[21]. Note that the approach presented here does not require computation of an optimal state and, thus, is better suited for real-time implementation.

For each gust intensity, a controller is computed by taking the mean value of nominal airspeed and gains for the last 20 generations. This is shown in Table 3. Since the longitudinal gust velocity is zero, gains relating to horizontal gusts have been set to 0.

Examining the gust-related gains ($K_{w,2}$) shows that an upward gust component (negative value of w_z) will induce a trailing edge up deflection of the elevator. This matches heuristics stated by Lissaman: climb in updrafts, dive in downdrafts (summarized as "belly to the wind"[18]). Gains related to gust gradient ($K_{w,4}$) show more variability, but are generally positive. This indicates a desire to accelerate through an upwards gradient. Thus, a strong upward gradient will induce a downward elevator deflection against the up deflection induced by upward components of wind. This tendency to accelerate through strong upward gradients also was observed in previous work[21] and matches results of a derivation presented by Lawrance[27]. However, gradients for this sinusoidal wind field are fairly low and, thus, do not have a strong impact on energy extraction.

Control design was repeated for Dryden gust spectra with w_{20} varying from 0.1 m/s to 14 m/s (28 knots, or a moderate wind). Flying altitude was 50m (164 feet). Together w_{20} and altitude determine the gust spectrum. Vertical and longitudinal gusts are considered simultaneously.

Results of nominal flying speed and energy extraction are shown in Figure 4. As with the sinusoidal gust field, increasing gust intensity results in higher nominal airspeed and greater energy extraction. Not surprisingly, convergence is significantly "rougher", since a different gust spectrum is used at each generation. However, an increase in energy change is still observed over the first 15 generations, indicated improving overall performance as the population evolves.

Again, for each gust intensity, a controller is computed from the mean value of the best nominal airspeed and gains over the last 20 generations. Results are tabulated in Table 4.

The largest root mean square vertical gust velocity is approximately 1 m/s. Energy change for this gust velocity is -0.09646 m/s^2, a factor of 2 better than the sinusoidal gust of this intensity. This is due, in part, to the larger gradients in the Dryden gust field compared with the sinusoidal gust field (the rms gradient is an order of magnitude larger for a given rms velocity), but may be in part due to the longitudinal gust components. This improvement in energy extraction for the Dryden gust over sinusoidal gusts also was observed by Patel for vertical-only gusts[25].

As with the sinusoidal gust fields, examining the gust-related gains $\mathbf{K}_w$ shows a tendency to climb in upwards gusts. Now, however, one also can see a tendency to climb in upwards gradients. The longitudinal gains $K_{w,1}$ and $K_{w,3}$ are generally negative, indicating a tendency to climb when a head wind gust is encountered (trading increased airspeed for altitude).

Effectiveness of gust soaring control

Monte Carlo simulations were used to assess the effectiveness of the gust soaring controllers discussed in the previous section (simulation results are based on the RnR products SB-XC radio control glider, see Apprndix). Four sets of simulations through Dryden gust fields with w_{20} equal to 2 m/s, 6 m/s, 10 m/s and 14 m/s were performed, with 100 instances of random gust fields done for each set. Three controllers were tested for each run: the full gust soaring controller (selected from Table 4 for the relevant wind condition); a vertical gust-only controller, where the horizontal gust gains in $\mathbf{K}_w$ were set to zero; and a state tracking controller, where all the gust-related gains were set to zero. The state to be tracked is a trimmed, steady glide at the nominal airspeed for the particular gust condition. This allows direct comparison of the full gust-soaring controller with a standard controller and allows an assessment of the effect of horizontal gusts on energy harvesting. Note, that for each controller, the full Dryden gust field (incorporating vertical and horizontal wind) was used.

Results are summarized in Figure 5. For each gust condition, bars show the minimum, maximum, average and standard deviations of the energy change per unit distance travelled for each controller. In all cases the gust soaring controllers outperformed the state tracking controller, with the margin increasing as the gust intensity increased. Further, the full gust soaring controller shows better performance than the vertical-only controller, indicating that energy can be extracted from horizontal gusts. Again, the margin increased as gust intensity increased. In fact, for every run both gust soaring controllers out-performed the state tracking controller and the full controller outperformed the vertical-only controller. For the w_{20}=10 case, the vertical only controller reduced energy loss by about 33% and the full gust controller reduced energy loss by about 40%. For the w_{20}=14 case (moderate turbulence), the vertical only controller reduced energy loss by about 41% and the full gust controller reduced energy loss by about 68%.

Detailed results from a single representative run with w_{20} equal to 10 m/s are presented in Figure 6. The total energy loss for the gust soaring controller is approximately 60% of the total energy loss for the state tracking controller, a 40% improvement in performance. The elevator inputs for the gust soaring controller are significantly greater, thus careful design of the control surfaces and actuation system may be necessary to reduce the energy required for actuation.

Some insight can be obtained by examining results of a flight through a sinusoidal gust (vertical only). Figure 7 shows a case with $\sigma_z = 1$ m/s, where the appropriate gain and speed to fly is selected from Table 3. Again, for the state tracking controller gust related gains are set to zero. The gust soaring controller shows less than half the energy loss of the state tracking controller. Close examination of $\frac{\Delta E}{\Delta x}$ shows that the greatest difference occurs during the downward gust: significantly less energy is lost during the down gust when using the gust soaring controller.

Conclusions

This paper has presented a control architecture for gust energy extraction that superimposes gust-dependent control inputs on control inputs required to maintain a trimmed, steady glide. A genetic algorithm is used to compute the nominal speed and control gains to maximize energy gain (or equivalently, minimize energy loss) over a specified distance.

Controllers for both sinusoidally varying vertical gusts and a vertical/longitudinal Dryden gust were designed. The nominal speed and control gains were found to depend on the gust intensity, with increasing gust intensity leading to greater airspeed and greater energy extraction. Designing a controller to extract energy from horizontal as well as vertical gusts improves performance. And, comparisons with state tracking controllers show that significant improvement in energy extraction is possible when gust soaring is employed.

References

[1]Boslough, M. B. E., "Autonomous Dynamic Soaring Platform for Distributed Mobile Sensor Arrays," Tech. Rep. SAND2002-1896, Sandia National Laboratories, 2002.

[2]Kiceniuk, T., "Calculations on Soaring in Sink," *Technical Soaring*, Vol. 25, No. 4, October 2001, pp. 228-230.

[3]Allen, M. J. and Lin, V., "Guidance and Control of an Autonomous Soaring Vehicle with Flight Test Results," *AIAA Aerospace Sciences Meeting and Exhibit*, AIAA Paper 2007-867, American Institute of Aeronautics and Astronautics, Reno, Nevada, January 2007.

[4]Phillips, W. H., "Propulsive Effects due to Flight through Turbulence," Journal of Aircraft, Vol. 12, No. 7, July 1975, pp. 624-626.

[5]MacCready Jr., P. B., "Optimum Airspeed Selector," *Soaring*, January-February 1958, pp. 10-11.

[6]Arho, R., "Distance Estimation Error and Stationary Optimal Gliding," *OSTIV Publication XII*, Organisation Scientifique et Technique Internationale du Vol a Voile, 1972.

[7]Metzger, D. E. and Hedrick, J. K., "Optimal Flight Paths for Soaring Flight," *Journal of Aircraft*, Vol. 12, No. 11, 1975, pp. 867-871.

[8]de Jong, J. L., "The Convex Combination Approach: A Geometric Approach to the Optimization of Sailplane Trajectories," *OSTIV Publication XVI*, Organisation Scientifique et Technique Internationale du Vol aVoile, 1981, pp. 182-201.

[9]Cochrane, J. H., "MacCready Theory with Uncertain Lift and Limited Altitude," *Technical Soaring*, Vol. 23, No. 3, July 1999, pp. 88-96.

[10]Irving, F., "The Energy Loss in Pitching Manoeuvres," *Proceedings of the XVI OSTIV Congress*, Organisation Scientifique et Technique Internationale du Vol a Voile, 1978.

[11]Gedeon, J., "The Influence of Sailplane Performance and Thermal Strength on Optimal Dolphin-Flight Transition Piloting Techniques," *Proceedings of the XV OSTIV Congress*, Organisation Scientifique et Technique Internationale du Vol a Voile, 1976.

[12]Gedeon, J., "Dynamic Analysis of Dolphin Style Thermal Cross Country Flight," *Proceedings of the XIV OSTIV Congress*, Organisation Scientifique et Technique Internationale du Vol a Voile, 1974.

[13]Zhao, Y. J., "Optimal Patterns of Glider Dynamic Soaring," *Optimal Control Applications and Methods*, Vol. 25, No. 2, 2004, pp. 67 -89.

[14]Zhao, Y. J. and Qi, Y. C., "Minimum Fuel Powered Dynamic Soaring of Unmanned Aerial Vehicles Utilizing Wind Gradients," *Optimal Control Applications and Methods*, Vol. 25, No. 5, 2004, pp. 211-233.

[15]Sachs, G. and Mayrhofer, M., "Shear Wind Strength Required for Dynamic Soaring at Ridges," *Technical Soaring*, Vol. 25, No. 4, October 2001, pp. 209-215.

[16]Sachs, G., "Minimum Shear Wind Strength Required for Dynamic Soaring of Albatrosses," *Ibis*, Vol. 147, 2005, pp. 1-10.

[17]Pennycuick, C. J., "Gust Soaring as a Basis for the Flight of Petrels and Albatrosses (Procellariiformes)," *Avian Science*, Vol. 2, No. 1, 2002, pp. 1-12.

[18]Lissaman, P., "Wind Energy Extraction by Birds and Flight Vehicles," *43rd AIAA Aerospace Sciences Meeting and Exhibit*, AIAA Paper 2005-241, American Institute of Aeronautics and Astronautics, Reno, Nevada, January 2005.

[19]Patel, C. K. and Kroo, I., "Control Law Design for Improving UAV Performance using Wind Turbulence," *AIAA Aerospace Sciences Meeting and Exhibit*, AIAA Paper 2006-0231, American Institute of Aeronautics and Astronautics, Reno, Nevada, January 2006.

[20]Lissaman, P. B. S. and Patel, C. K., "Neutral Energy Cycles for a Vehicle in Sinusoidal and Turbulent Vertical Gusts," *45th AIAA Aerospace Sciences Meeting and Exhibit*, AIAA Paper 2007-863, American Institute of Aeronautics and Astronautics, Reno, Nevada, January 2007.

[21]Langelaan, J. W. and Bramesfeld, G., "Gust Energy Extraction for Mini- and Micro- Uninhabited Aerial Vehicles," *46th AIAA Aerospace Sciences Meeting and Exhibit*, AIAA Paper 2008-0223, American Institute of Aeronautics and Astronautics, Reston, Virginia, January 2008.

[22]Gorisch, W., "Energy Exchange between a Sailplane and Moving Air Masses under Nonstationary Flight Conditions with respect to Dolphin Flight and Dynamic Soaring," *Proceedings of the XV OSTIV Congress*, Organisation Scientifique et Technique Internationale du Vol a Voile, 1976.

[23]Thrun, S., Fox, D., and Burgard, W., *Probabilistic Robotics*, MIT Press, September 2005.

[24]Hoblit, F. M., *Gust Loads on Aircraft: Concepts and Applications*, AIAA Education Series, American Institute of Aeronautics and Astronautics, Reston, Virginia, 1988.

[25]Patel, C. K., *Energy Extraction from Atmospheric Turbulence to Improve Aircraft Performance*, VDM Verlag Dr. Muller, Saarbruken, 2008.

[26]Military Specification, "Flying Qualities of Piloted Airplanes," *Tech. Rep. MIL-F-8785C*, November 1980.

[27]Lawrance, N. and Sukkarieh, S., "Wind Energy Based Path Planning for a Small Gliding Unmanned Aerial Vehicle," *Proceedings of the AIAA Guidance, Navigation and Control Conference*, Chicago, Illinois, August 2009.

[28]Pachter, M., Ceccarelli, N. and Chandler, P. R., "Estimating MAV's Heading and the Wind Speed using GPS, Inertial and Air Data Measurements," *AIAA Guidance, Navigation and Control Conference*, AIAA Paper 2008-6311, American Institute of Aeronautics and Astronautics, Reston, Virginia, August 2008.

[29]Myschik, S., Heller M. Holzapfel, F. and Sachs, G., "Low-cost Wind Measurement System for Small Aircraft," *AIAA Guidance, Navigation and Control Conference*, AIAA Paper 2004-5240, American Institute of Aeronautics and Astronautics, Reston, Virginia, August 2004.

Appendix: Aircraft properties

Simulation results are based on the RnR products SB-XC radio control glider. Parameters in Table 1 were obtained from a drag buildup computation; state limits in Table 2 were defined to limit states to "reasonable" bounds.

Note that a fourth order polynomial is used to relate C_D to C_L; this provided a better fit to the computed data over the full speed range.

Table 1
Properties of SB-XC glider

variable	value	description
M	10 kg	mass
B	4.34 m	wing span
C	0.232 m	MAC
S	1 m^2	wing area
I_{yy}	1.87 kgm^2	
C_{L0}	0.37	
C_{L_α}	5.54 /rad	
C_{L_Q}	-3.255 s/rad	
$C_{L_{\dot\alpha}}$	-0.651 s/rad	
$C_{L_{\delta_e}}$	-0.37 /rad	
$C_{L_{\delta_f}}$	1.63 /rad	
$f_{L/D}(\phi)$	$0.1723\phi^4 - 0.3161\phi^3 + 0.2397\phi^2 - 0.0624\phi + 0.0194$	where $\phi = C_{L0} + C_{L_\alpha}\alpha$
$C_{D_{\delta_e}}$	0 /rad	
$C_{D_{\delta_f}}$	0.042 /rad	
C_{m0}	0	
C_{m_α}	-1.02 /rad	
C_{m_Q}	-14.6 s/rad	
$C_{m_{\delta_e}}$	1.6275 /rad	
$C_{m_{\delta_f}}$	-0.254 /rad	

Table 2
State limits and control saturation SB-XC glider

state/ control	range	Description
θ	$[-45^\circ \quad 45^\circ]$	Pitch
v_a	[11 m/s 35 m/s]	air speed
α	$[-2^o \quad 12^o]$	angle of attack
Q	[–999 rad/s 999 rad/s]	pitch rate
δ_e	$[-20^o \quad 20^o]$	elevator deflection

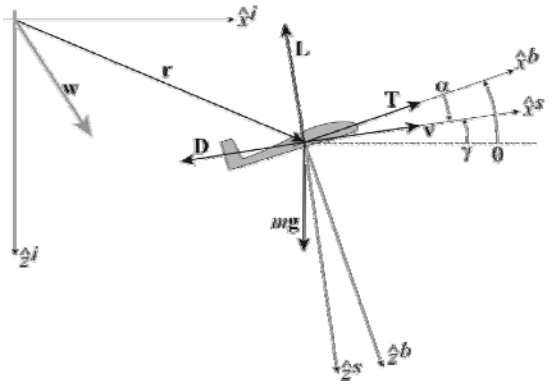

Figure 1 Reference frames. Positive rotations are indicated, so positive glide slope is upwards and angle of attack is positive in the conventional sense.

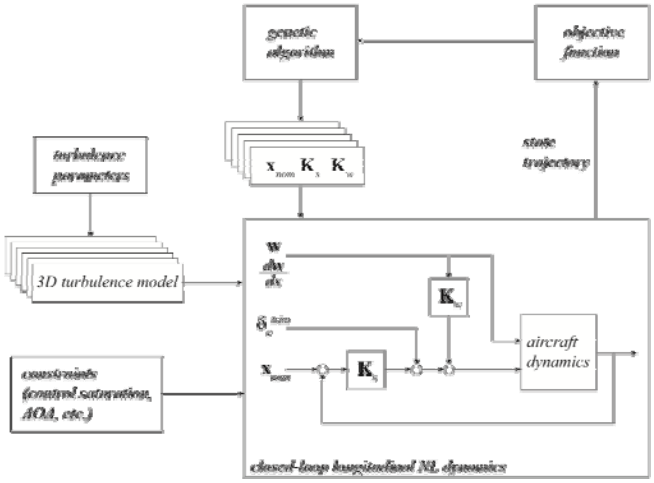

Figure 2 Genetic algorithm based design process for finding control gains.

Editor's note: Figures 3, 4, 6 and 7 contain colors. Please see the online paper to view the colors (journals.sfu.ca/ts/).

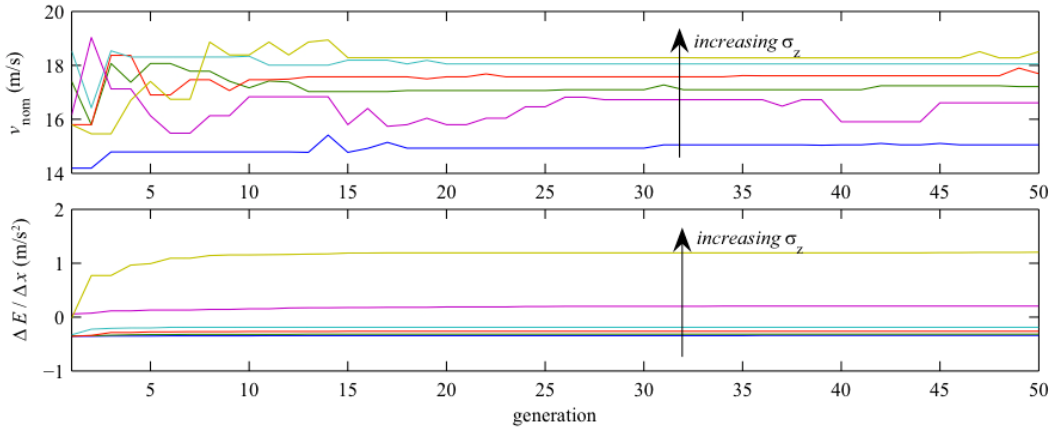

Figure 3 Best flight speed and energy change for flight through sinusoidal gust fields. Each curve represents a different root-mean-square vertical velocity. Energy change in still air is approximately -0.38m/s^2.

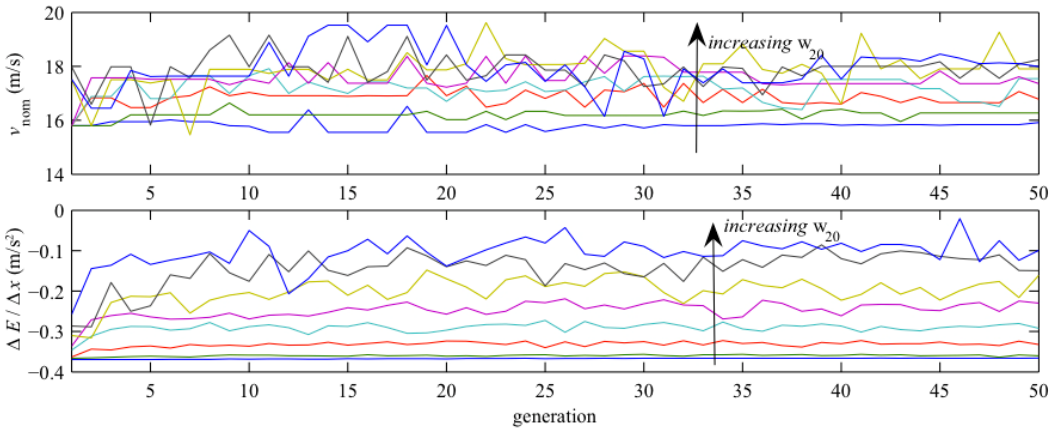

Figure 4 Best flight speed and energy change through Dryden gust fields. Each curve represents a different w_{20}. Energy change in still air at best L/D is approximately -0.38 m/s^2.

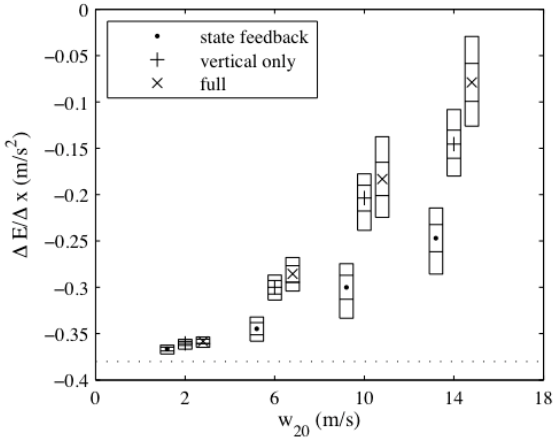

Figure 5 Summary of Monte Carlo simulation of flight through Dryden gust fields. Three controllers are compared: state feedback only, vertical gust only, and full gust control. Results show the mean energy change (symbol); bars show the minimum, maximum and 1σ bounds on energy change. The dotted line at -0.38 shows the energy change in a steady glide in still air.

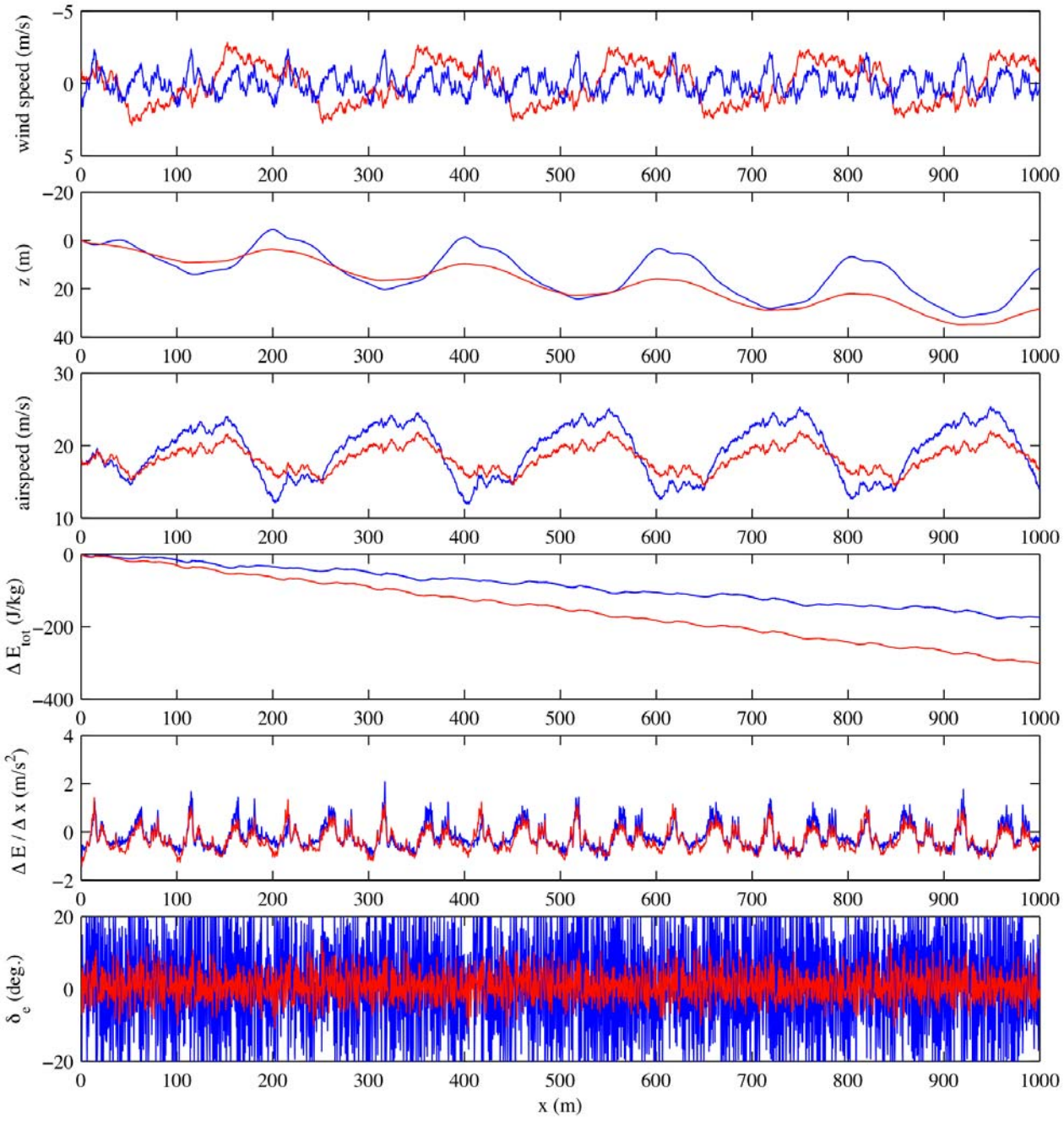

Figure 6 Comparison of gust soaring control and state feedback-only control for vertical/longitudinal Dryden gust. The upper plot shows gust velocity (longitudinal in red, vertical in blue). For the remaining plots blue denotes the gust soaring controller and red denotes the state tracking controller.

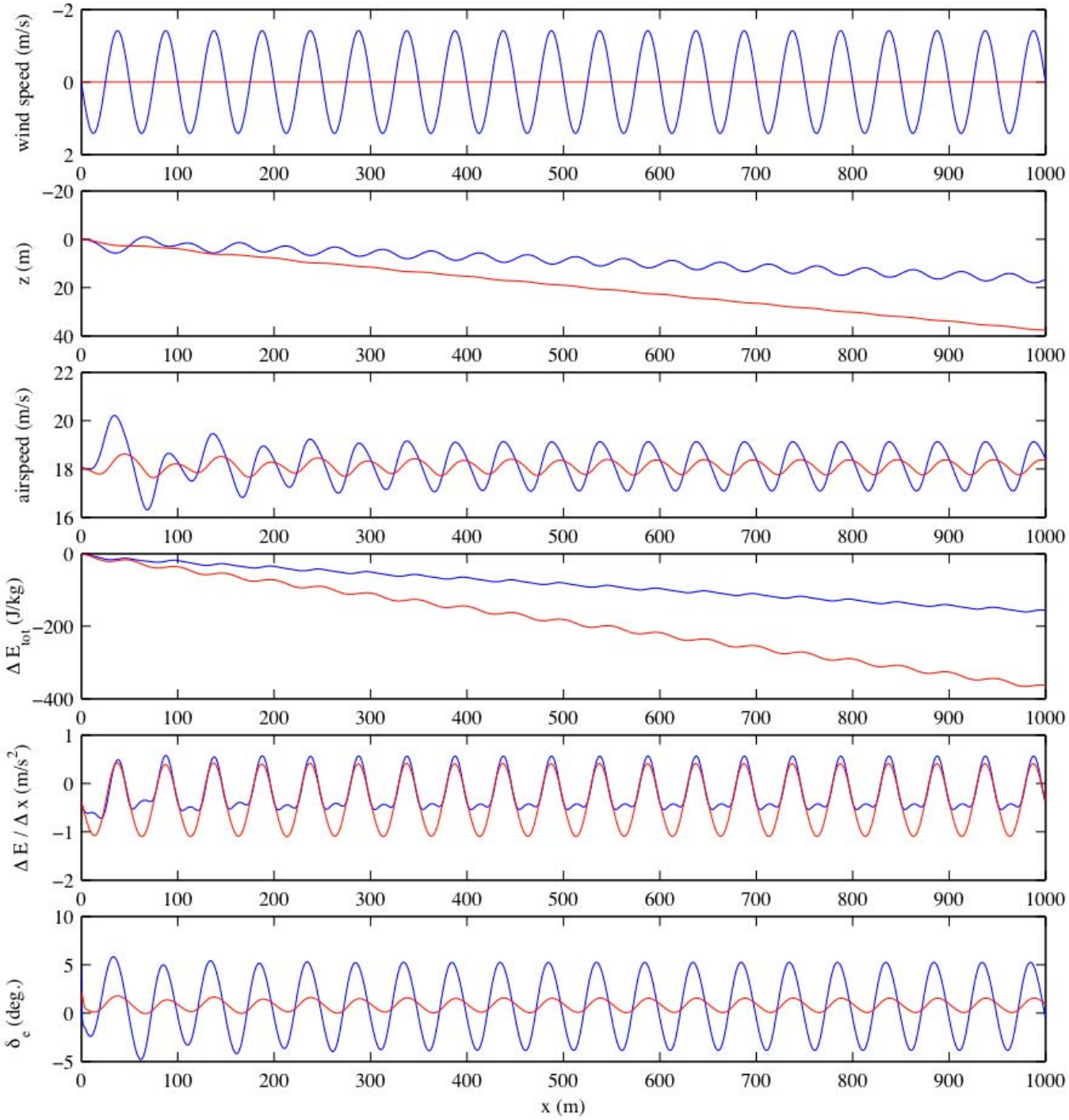

Figure 7 Comparison of gust soaring control and state feedback-only control for a vertical sinusoidal gust. The upper plot shows gust velocity (longitudinal in red, vertical in blue). For the remaining plots blue denotes the gust soaring controller and red denotes the state tracking controller.

Table 3
Vertical sinusoid gust controllers, wavelength=50m. Energy change in still air at best L/D is approximately -0.38 m/s^2.

rms	$\frac{\Delta E}{\Delta x}$	$v_{a,nom}$	$\mathbf{K}_s$	$\mathbf{K}_w$
(m/s)	(m/s^2)	(m/s)		
0.01	-0.343	15.1	[0.03236 0.3865 5.615 3.199]	[0 –3.532 0 2.637]
0.5	-0.319	17.2	[–0.6966 –0.9084 2.079 6.090]	[0 –2.341 0 –2.632]
0.75	-0.264	17.6	[0.436 –0.1239 7.772 0.3923]	[0 –0.600 0 0.2395]
1	-0.190	18.06	[0.5173 –0.1846 5.512 0.5847]	[0 –0.4065 0 0.3913]
2	0.202	16.48	[2.365 –0.1268 2.725 5.052]	[0 –0.1519 0 2.203]
4	1.194	18.3	[0.9703 –0.0265 5.228 0.5847]	[0 –0.1689 0 0.7221]

Table 4
Dryden gust controllers, altitude 50m. Energy change in still air at best L/D is approximately -0.38 m/s^2.

w_{20}	$rms(w_x)$	$rms(w_z)$	$\frac{\Delta E}{\Delta x}$	$v_{a,nom}$	gains
(m/s)	(m/s)	(m/s)	(m/s^2)	(m/s)	
0.1	0.014	0.0076	-0.3662	15.84	$\mathbf{K}_s = [-0.507 \quad -0.0277 \quad 5.485 \quad 0.4538]$ $\mathbf{K}_w = [0.0968 \quad -0.1617 \quad -1.038 \quad -0.2678]$
2	0.2764	0.1513	-0.3588	16.27	$\mathbf{K}_s = [3.015 \quad -0.03072 \quad 6.078 \quad 2.365]$ $\mathbf{K}_w = [-0.5235 \quad -1.949 \quad -0.1159 \quad -2.12]$
4	0.5517	0.303	-0.3298	16.79	$\mathbf{K}_s = [0.7077 \quad 0.00115 \quad 5.902 \quad 1.141]$ $\mathbf{K}_w = [-0.1309 \quad -1.158 \quad 0.1173 \quad -0.8445]$
6	0.8239	0.4537	-0.2889	17.18	$\mathbf{K}_s = [1.382 \quad -0.0277 \quad 4.338 \quad 1.814]$ $\mathbf{K}_w = [-0.2185 \quad -1.173 \quad -0.1433 \quad -0.7241]$
8	1.117	0.6135	-0.2398	17.53	$\mathbf{K}_s = [0.9158 \quad -0.03579 \quad 5.351 \quad 2.243]$ $\mathbf{K}_w = [-0.143 \quad -0.122 \quad -0.3297 \quad -0.6711]$
10	1.4	0.7683	-0.1961	17.93	$\mathbf{K}_s = [0.9317 \quad -0.0277 \quad 5.628 \quad 1.137]$ $\mathbf{K}_w = [-0.1354 \quad -0.619 \quad -0.34 \quad -0.2378]$
12	1.669	0.9169	-0.1214	17.84	$\mathbf{K}_s = [0.8398 \quad -0.0277 \quad 5.351 \quad 1.532]$ $\mathbf{K}_w = [-0.1064 \quad -0.6197 \quad -0.01912 \quad -0.06805]$
14	1.956	1.073	-0.09464	17.86	$\mathbf{K}_s = [1.657 \quad -0.0277 \quad 5.426 \quad 0.8405]$ $\mathbf{K}_w = [-0.1458 \quad -0.3333 \quad -0.06309 \quad 0.1572]$